WHITE PAPER 30767

Clumped isotope analysis of methane using HR-IRMS:

New insights into origin and formation mechanisms of natural gases and a potential geothermometer

Authors: Guannan Dong, Hao Xie, John Eiler, California Institute of Technology, Pasadena, USA; Naizhong Zhang, Mayuko Nakagawa, Naohiro Yoshida, Earth-Life Science Institute, Tokyo Institute of Technology, Tokyo, Japan; Daniel Eldridge, Daniel Stolper, University of California, Berkeley, USA; Nina Albrecht, Issaku E. Kohl, Thermo Fisher Scientific, Bremen, Germany

Keywords: HR-IRMS, methane, clumped isotopes, $^{12}CH_2D_2$, $^{13}CH_3D$, geothermometry, reaction kinetics, natural gas, petroleum geochemistry

Goal

This white paper describes the analytical capabilities of the Thermo Scientific™ Ultra™ High Resolution Isotope Ratio Mass Spectrometer (HR-IRMS) for the analysis of doubly substituted isotopologues ('clumped isotopes') of methane, including both $^{13}CH_3D$ and $^{12}CH_2D_2$, and for analysis of the $\delta^{13}C$ and δD signatures of methane with exceptional precision.

Introduction

Methane (CH_4) is widely distributed in the solid earth, ocean and atmosphere. It is a primary constituent of geological gas deposits and a significant resource for global energy production; the fact that it generates less CO_2 per unit energy on combustion means its expanded use over recent decades has been a significant factor in mitigating the rate of rise of atmospheric greenhouse gases. In addition to its commercial importance, it plays a major role in the global carbon cycle and is involved in various fluxes within atmospheric, microbial, hydrothermal and magmatic systems. It even has potential to be utilized as an extraterrestrial biosignature. Methane is also amongst the most effective greenhouse gases and as a result could play a significant role in the anthropogenic acceleration of climate change.

The importance and versatility of methane fuels the development of methods to decipher its origins, sources and sinks, formation conditions, and transport paths.

Berkeley UNIVERSITY OF CALIFORNIA Caltech

ThermoFisher SCIENTIFIC

The isotopic composition of methane is a valuable tool to address these questions. The commonly measured isotope compositions, $\delta^{13}C$ and δD, are determinable by combining chemical transformations (via combustion/pyrolysis to CO_2 or H_2, respectively) with classical low-resolution IRMS. Such measurements can aid in identification of methane's origins but are often ambiguous with respect to provenance and formation conditions because multiple formation pathways can lead to broadly similar bulk isotope contents. The 'clumped isotope' signatures, $\Delta^{13}CH_3D$ and $\Delta^{12}CH_2D_2$, add additional independent compositional dimensions, which improve forensic identification, recognition of methane's formation mechanisms, and have the potential to record the absolute formation temperature of methane in cases where the natural gas formed in internal thermodynamic equilibrium (i.e., the clumped isotope composition can be utilized as a geothermometer).

Both bulk and clumped isotope signatures can be directly determined with high precision using the Ultra HR-IRMS.

Conventional stable isotope systematics of methane ($\delta^{13}C$ and δD)

The molecule-average (or 'bulk') stable isotope characteristics of methane, $\delta^{13}C$ and δD, are utilized to distinguish between (1) thermogenic methane (formed by thermal degradation of buried organic matter), (2) biogenic methane (formed by microbial metabolism), and (3) abiotic methane (formed inorganically, typically by water-rock reaction). Thermogenic, microbial, and abiotic mechanisms can potentially be distinguished by measurements of $\delta^{13}C$ and δD because these processes draw on isotopically distinct substrates, and because isotopic fractionations associated with these processes differ from one another. However, large variations are observed in the resulting isotopic signatures of each process due to variations in substrate isotopic content and in the progress or conditions of reactions. As a result, the three major methane types occupy overlapping fields in a plot of $\delta^{13}C$ vs. δD (Figure 1). Moreover, natural accumulations of methane are frequently mixtures of two or more sources and thus can occupy positions in Figure 1 intermediate between the various extremes. For these reasons, only the most extreme $\delta^{13}C$ and δD signatures can reliably identify the sources of natural methane. Perhaps most problematically, most natural methane accumulations are thermogenic, and thus occupy positions in Figure 1 that could be explained by mixtures of any number of other sources. Finally, even when a methane falls in a field in Figure 1 unique to one origin, the isotopic signature does not directly record other information of potential interest, such as formation temperature.

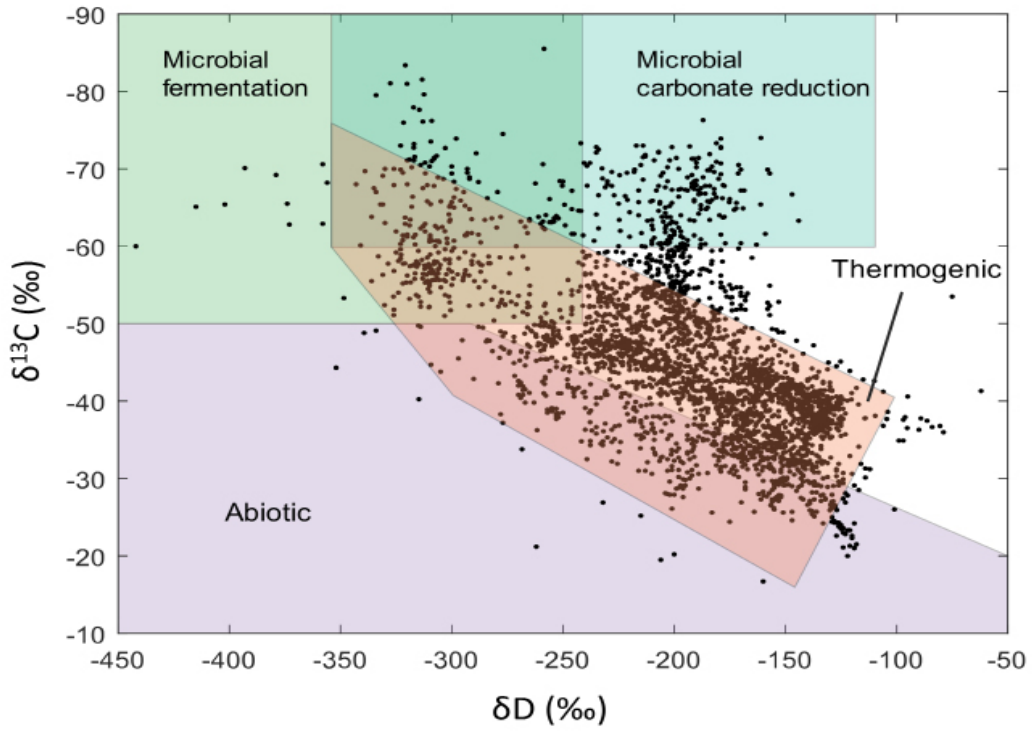

Figure 1. Values of $\delta^{13}C$ vs. δD for methane from diverse sources. Note that natural variations can be associated with ranges characteristic of several formation processes, but data for each type spans ranges that partly overlap fields for one or more others. Modified based on Douglas et al. (2017), Etiope (2015), Etiope & Sherwood Lollar (2013), Milkov and Etiope 2018, Schoell (1980), Sherwood et al. (2017), Thiagarajan et al. (2020).

Clumped isotope systematics of methane

The doubly substituted (or 'clumped') isotopologues of methane, $^{13}CH_3D$ and $^{12}CH_2D_2$, provide two new independent constraints that can resolve ambiguities in its provenance and add fresh tools for understanding the environments and chemical mechanisms of natural methane formation. Abundances of the clumped isotopic species are influenced by the same chemical, physical and biological processes that control $\delta^{13}C$ and δD (Figure 1), but differences between the fractionation behaviors of each unique isotopologue ($^{13}CH_4$, $^{12}CH_3D$, $^{13}CH_3D$, $^{12}CH_2D_2$) create new opportunities to distinguish those processes from one another. Moreover, the proportions of 'clumped' isotopic species can be sensitive to environmental factors that are otherwise unconstrained by conventional methane stable isotope measurements (i.e., $\delta^{13}C$ and δD) alone; most notably, in methane that has formed in thermodynamic equilibrium with its surroundings, the clumped isotope composition provides a direct and absolute measurement of formation temperature (Figure 2; data obtained with the Ultra HR-IRMS at UC Berkeley).

The potential of clumped isotope measurements to illuminate the origins of methane are illustrated in Figure 3, which plots the excesses, relative to a stochastic distribution of all isotopes among all possible methane isotopologues, of the two doubly substituted species, i.e., the $\Delta^{12}CH_2D_2$ value vs. the $\Delta^{13}CH_3D$ value (see Eiler (2007) and Eldridge et al. (2019) for a general explanation and further details regarding the Δi nomenclature). A sample that plots at the origin of this figure possesses concentrations of $^{13}CH_3D$ and $^{12}CH_2D_2$ exactly equal to what would be expected if all ^{13}C and D in that sample were randomly distributed among all possible isotopic forms of methane. The upward-concave curve represents the set of compositions that would be observed in methanes that have obtained a distribution of isotopes among isotopologues consistent with isotope exchange equilibrium at a given temperature, i.e., the line of simultaneous consistency with the trends on the left and right panels of Figure 2 (note the temperatures of equilibrium marked on the curve in Figure 3). Simple kinetically controlled processes, such as gas phase diffusion, also lead to distinctive enrichments and depletions in the multiply substituted species (dashed arrows in Figure 3). Finally, more complex kinetically controlled methane formation mechanisms, such as pyrolysis of aliphatic hydrocarbons (red arrow), biological hydrogenotrophic CO_2 reduction (green curved field) and abiotic CO_2 reduction (purple rectangle), are associated with distinctive fractionations that also depart from the equilibrium curve in Figure 3. In cases where the combination of $\delta^{13}C$, δD and clumped isotope

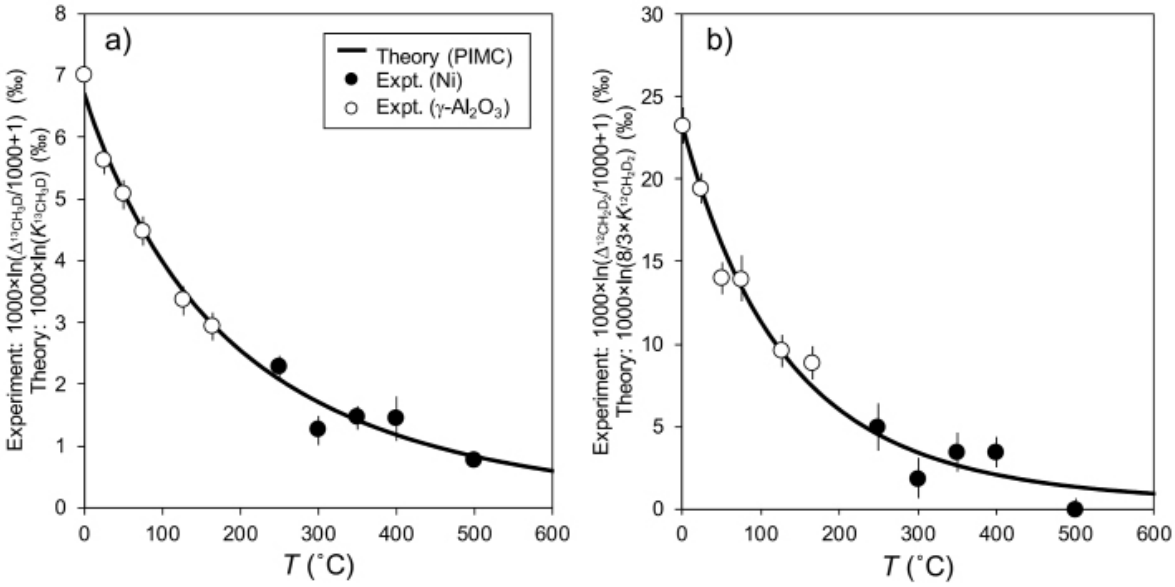

Figure 2. Plots of the equilibrium constants for the reactions $^{13}CH_4 + {}^{12}CH_3D = {}^{12}CH_4 + {}^{13}CH_3D$ (panel a) and $2x^{12}CH_3D = {}^{12}CH_4 + {}^{12}CH_2D_2$ (panel b), vs. temperature of equilibrium. The multiply substituted species are energetically favorable, driving equilibrium constants to values higher than the stochastic mass action constant for each reaction, because of their exceptionally slow rates of intramolecular vibrations. As a result, the multiply substituted species form in excess of their stochastic proportions in equilibrated systems, by relatively large amounts at low temperatures and smaller amounts at high temperatures. Modified after Eldridge et al. (2019).

abundances leads to a confident identification of the formation process, one can often reach conclusions about the isotopic compositions of the substrates utilized during methanogenesis, further constraining the environment of formation.

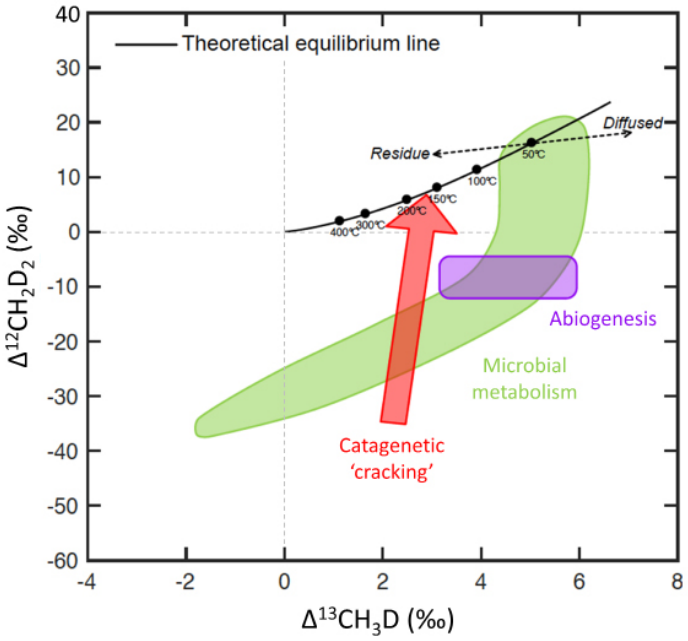

Figure 3: Schematic illustration of the clumped isotope signatures associated with mutual thermodynamic equilibrium among all methane isotopologues (solid black curve, marked with corresponding temperatures of equilibrium), gas phase diffusion (dashed line), catagenetic 'cracking' of aliphatic precursors (red arrow, pointing from low to high thermal maturity), microbial production by CO2 reduction (green curved field) and abiotic formation on metal catalysts (purple rectangle).

Our understanding of how these mechanisms affect clumped isotopologue abundance and distribution suggest three ways in which they can be used to study the origins of methane:

1. Improved forensic discrimination between the major methane types, i.e., based on the fact that a four-dimensional composition space ($\delta^{13}C$ vs. δD vs. $\Delta^{12}CH_2D_2$ vs. $\Delta^{13}CH_3D$) offers better separation between compositional types than two dimensions alone (Figure 1);
2. Recognition of specific chemical mechanisms of methanogenesis (i.e., through matching of sample data to known trends in Figure 3)
3. Quantitative geothermometry (i.e., based on the specific location of an equilibrated sample along the equilibrium curves in Figure 2 and Figure 3). A later section of this report utilizes case studies based on data from Caltech and UC Berkeley Ultra laboratories to provide additional detail on how each of the above approaches are applied.

Instrumentation

The Ultra HR-IRMS is a double-focusing, multi-collector gas source isotope ratio mass spectrometer. The system employs ion counters and is optimized, both in detector sensitivity and analyzer abundance sensitivity, for the detection of exceptionally rare isotope species, such as clumped isotopologues. Mass resolving powers beyond 30,000 (5%, 95% edge definition; reaching up to 50,000 for some applications) enable the separation of isobaric interferences arising from ionization adducts, contaminants, fragments, and isotopologues of the analyte that share the same cardinal mass. This is key to analyzing interference-free signals of all singly and doubly substituted methane isotopologues at natural abundance levels. Such measurements are made more complex for methane and many other organic compounds by the fact that electron-impact ionization of such species at electron energies sufficient to produce abundant ions (typically ~70 eV) also lead to abundant formation of fragment ions (CH_3^+, CH_2^+, etc.) as well as hydrogen-adducts (CH_5^+). Thus, isotopic forms of several different chemical species often appear as families of closely spaced nearly isobaric interferences.

Table 1: Masses of the single and double substituted isotopologues of methane (bold), respective adducts, fragments, and typical contaminants. All species listed are fully resolvable with the Ultra HR-IRMS.

Cardinal mass	Ion species	Type	[amu]
16	$^{16}O^+$	Contaminant	15.9949
	$^{15}NH^+$	Contaminant	16.0079
	$^{14}NH_2^+$	Contaminant	16.0187
	$^{13}CH_3^+$	Fragment	16.0268
	$^{12}CH_4^+$	**Isotopologue**	**16.0313**
17	$^{17}O^+$	Contaminant	16.9991
	$^{16}OH^+$	Contaminant	17.0027
	$^{14}NH_3^+$	Contaminant	17.0266
	$^{13}CH_2D^+$	Fragment	17.0331
	$^{13}CH_4^+$	**Isotopologue**	**17.0347**
	$^{12}CH_3D^+$	**Isotopologue**	**17.0376**
	$^{12}CH_5^+$	Adduct	17.0391
18	$^{18}O^+$	Contaminant	17.9992
	$H_2{}^{16}O^+$	Contaminant	18.0106
	$^{13}CH_3D^+$	**Isotopologue**	**18.0409**
	$^{13}CH_5^+$	Adduct	18.0425
	$^{12}CH_2D_2^+$	**Isotopologue**	**18.0439**
	$^{12}CH_4D^+$	Adduct	18.0454

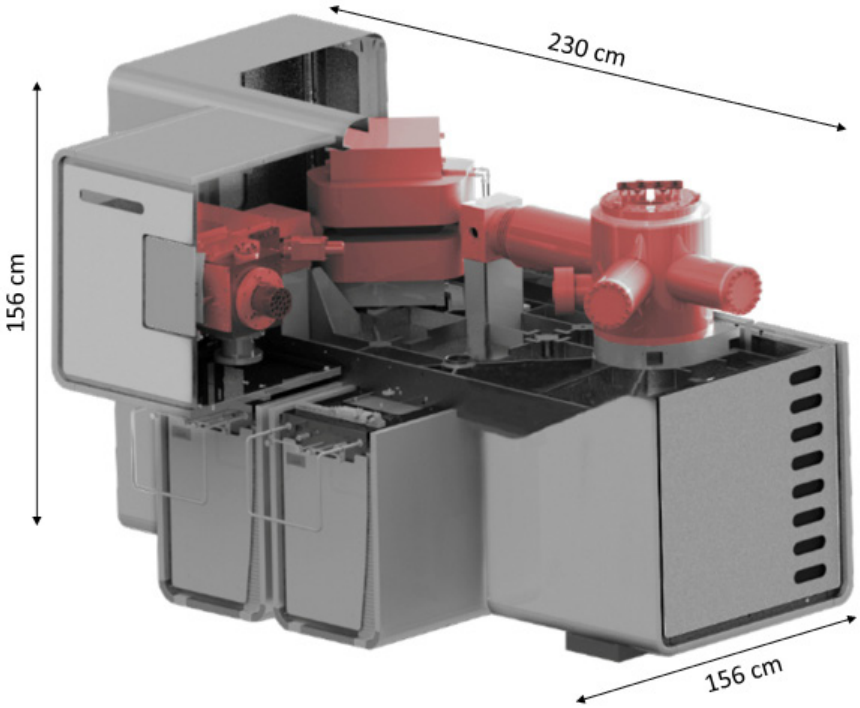

Figure 4a: Interior schematics of the Ultra HR-IRMS. All hardware components relevant to the guiding of the ion beam path (shaded in red) are mounted on a monolithic platform with a small footprint to guarantee maximum ion optical stability.

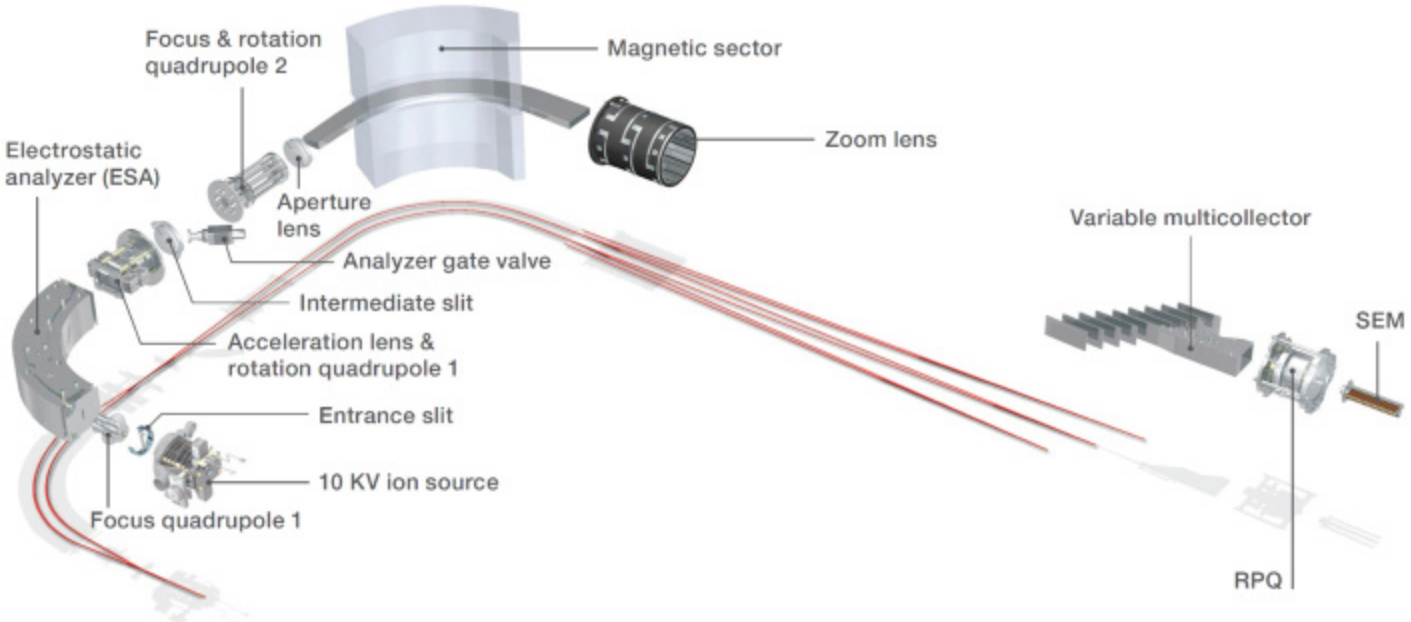

Figure 4b: Ultra HR-IRMS ion beam path. The electrostatic analyzer is followed by the magnetic sector in the double-focusing Nier-Johnson type mass analyzer. Ions are accelerated to full potential before reaching the intermediate slit. Three sets of electromagnetic lenses prior to the electrostatic and magnetic sectors control the focusing of the ion beam, a zoom lens enables adjustment of dispersion. Signals are detected in an automated, variable position multicollector equipped with 9 Faraday cups 8 of which are moveable. The multicollector employs 4 ion counters for the detection of smallest ion beams. Temperature-controlled hardware (HV electronics, magnet, amplifier housing) guarantee maximum electronic stability.

With HR-IRMS using the Ultra HR-IRMS (Figure 4a, 4b), all isotopologues of methane and its fragments and adducts are fully resolvable from each other and from potential adducts, fragments, and contaminants (Table 1).

Peak separation with high resolution

Full peak separation of methane isotopologues and respective adducts at mass 17 (Figure 5a) and mass 18 (Figure 5b) is routinely obtained in high resolution mode at mass resolving powers beyond 30,000 employing a narrow collector exit slit (accelerating voltage: 10 kV, source slit width: 5 µm, collector slit width: 40 µm) (cf. Figure 6, Panel 1). This is achieved by narrowing the ion beam, removing edge-effect related aberrations, and finally focusing the beam through a narrow collector slit. Further improvement is possible by using the aperture lens, which results in approximately 30% less transmission. Fine adjustment of the ion beam ('resolution tuning') is performed by adjusting two sets of focus quadrupoles along the beam path, to optimize the energy profile and trajectory of the ion beam.

Users typically achieve MRP >40,000 up to 50,000.

Figure 5c illustrates partial peak separation obtained in high resolution mode at mass resolving powers beyond 30,000 employing a standard collector slit (accelerating voltage: 10 kV, source slit width: 5 µm, collector slit width: 800 µm). Full peak separation is compromised in favor of higher transmission and reduced measurement time (cf. Figure 6, Panel 2).

In addition to the focus, the conditions within the ion source ('source tuning') are of crucial importance for the successful measurement of clumped methane isotopologues. Ion source parameters, such as the extraction potential, determine residence time of analyte molecules proximal to the electron beam, thereby controlling the formation and fragmentation rates in the sample gas. These parameters are balanced to maximize the intensity of the analyte ion beam while minimizing the formation of adducts.

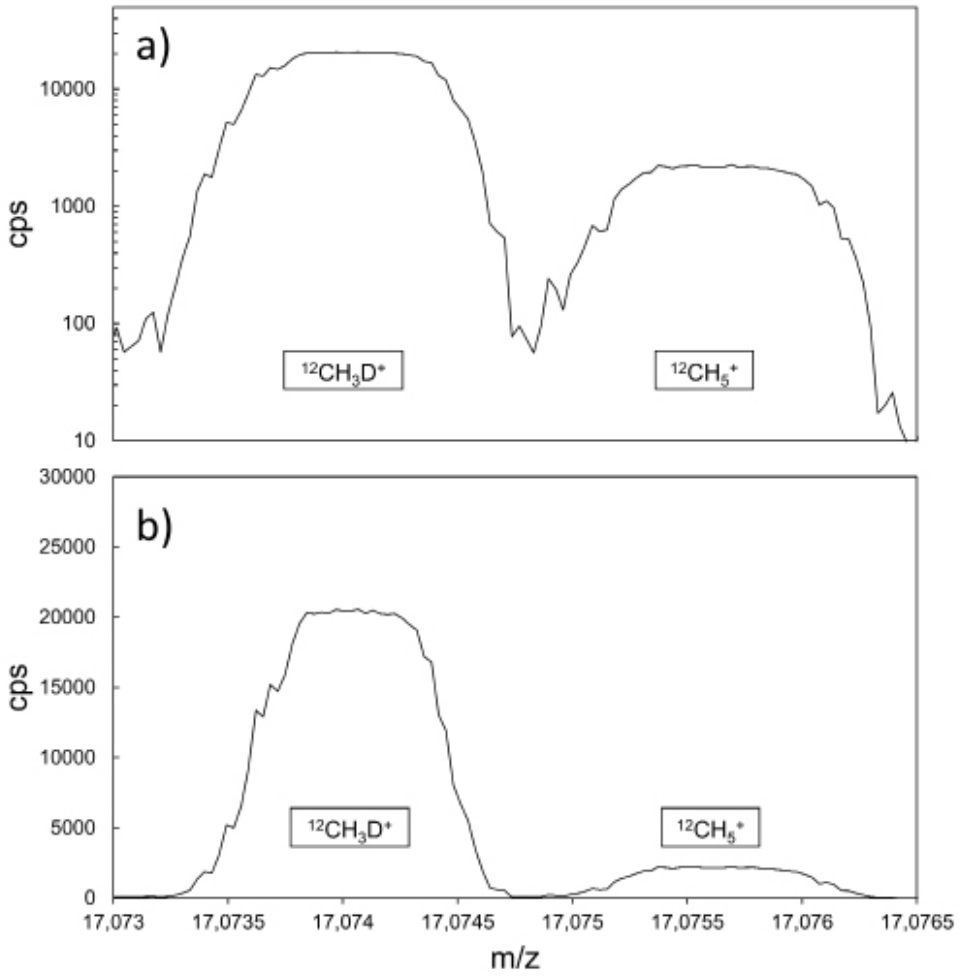

Figure 5a: Full peak separation for methane at mass 17 in high resolution mode with aperture and with a 40 µm collector slit, (a) logarithmic scale, (b) linear scale. Isotopologue and adduct are fully resolved. Mass resolving power ~45,000 (5%, 95% edge definition), statistically flat plateau of about 0.0004 *m/z*. Instrument mass stability is specified to 10 ppm, corresponding to ~0.0002 *m/z.*

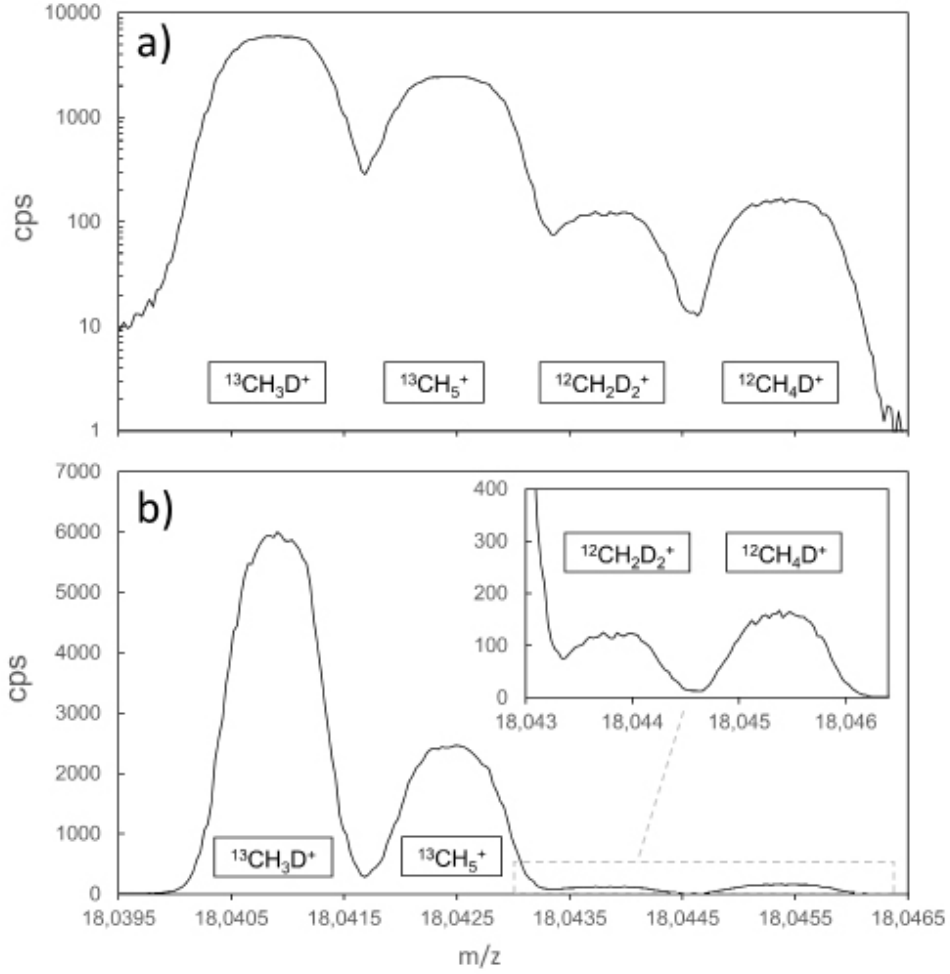

Figure 5b: Full peak separation for methane at mass 18 in high resolution mode without aperture and with a 40 µm collector slit, (a) logarithmic scale, (b) linear scale. Isotopologue and adduct are fully resolved. Mass resolving power ~45,000 (5%, 95% edge definition), statistically flat plateau of about 0.0004 *m/z*. Instrument mass stability is specified to 10 ppm, corresponding to ~0.0002 *m/z*.

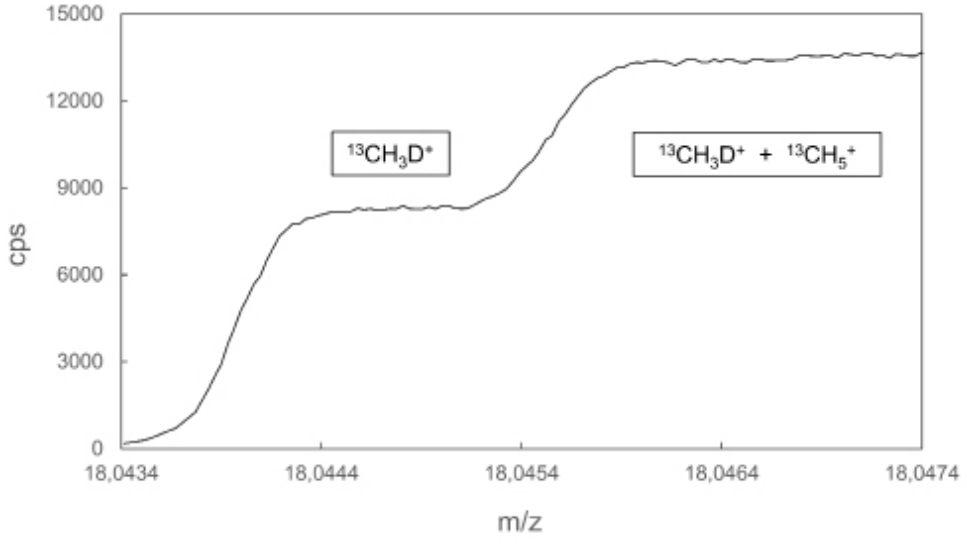

Figure 5c: Partial peak separation for methane at mass 18 with an 800 µm collector slit in high resolution mode without aperture. $^{13}CH_3D$ and $^{13}CH_5$ are partly resolved. Resolving power >30,000 (5%, 95% edge definition), statistically flat $^{13}CH_3D$-plateau of about 0.0007 *m/z*. Instrument mass stability is specified to 10 ppm, corresponding to ~0.0002 *m/z*.

Sensitivity

Useful ion yield is just below 0.1‰ or 1200:1 molecules/ion in full transmission, low resolution mode as measured for CO_2. This is around 50‰ of that observed for the Thermo Scientific™ 253 Plus™ 10 kV IRMS a reduction that is proportional to the low resolution slit width being 250 µm compared to the 500 µm for the 253 Plus IRMS. The further reduction in entrance slit width in medium and high-resolution modes results in a corresponding, linear decrease in ion yield, suggesting for all measured slit widths, beam density is homogeneous. Measurements of the isotopologue inventory of methane (cf. Figure 6) are performed in high resolution mode. Source pressure is typically adjusted to $2 \cdot 10^{-7}$ mbar, to obtain signal intensities in the range of 100 cps to 120 cps for the rare $^{12}CH_2D_2$ (Table 2).

Table 2: Typical intensities for the methane isotopologues of interest at a source pressure of about $2.0 \cdot 10^{-7}$ mbar purified methane in (high-resolution mode without aperture).

Molecule ion	$^{12}CH_4^+$	$^{13}CH_4^+$	$^{12}CH_3D^+$	$^{13}CH_3D^+$	$^{12}CH_2D_2^+$
Intensity [cps]	$1.5 \cdot 10^9$	$1.6 \cdot 10^7$	$7.0 \cdot 10^5$	$7.0 \cdot 10^3$	100 - 120

Sample preparation

The purification of natural gas samples can be achieved in two ways (or a combination of the two):

1. A sequence of repeated freezing and thawing using a liquid-helium cryostat and a vacuum apparatus. In this case, the sample is condensed at -253 °C, warmed to -228 °C while exposed to vacuum to remove less condensable gases (e.g. helium, hydrogen, oxygen, nitrogen) and finally warmed to -203 °C to release methane while retaining other hydrocarbons in the trap. Released pure methane is condensed onto a molecular sieve, which is then isolated and warmed to allow the methane to expand into the Dual Inlet system of the Ultra HR-IRMS. A detailed description of a methane purification procedure is described by e.g. Stolper et al. (2014a, 2014b), Eldridge et al. (2019).

2. Preparatory gas chromatography followed by capture of the isolated methane peak. A variety of architectures are possible for isolating methane from gas mixtures using gas chromatography (GC) and cryo-focusing. The critical components and workflows consist of (1) initial capture of the entire sample in a pre-evacuated volume containing a substrate (e.g. silica gel or molecular sieve at liquid nitrogen temperature), (2) warming up the sample while entraining it in a carrier gas (e.g. helium) enroute to the GC column, (3) accurate knowledge of elution times for methane from the GC column(s), (4) cryo-capture of eluted methane in a second volume containing substrate. This concentrated methane is then transferred to the Dual Inlet system of the mass spectrometer (e.g. Young et al., 2017).

Accurate mass spectrometric analyses of the methane isotopologues require high sample purity and in some cases sample purification by these methods must be done two or more times, or in combination. This is often the case when separating small amounts of methane from mixtures where methane is a minor component.

Data acquisition

Possible measurement strategies to access the full inventory of methane isotopologues, to derive both the molecule-average ($\delta^{13}C$ and δD) and clumped isotope ($\Delta^{13}CH_3D$ and $\Delta^{12}CH_2D_2$) compositions, are illustrated Figure 6.

Instrument stability and measurement precision

When measuring $\delta^{13}C$, $^{13}CH_4$ is acquired with a typical intensity of around $1 \cdot 10^7$ cps, which leads to noise limited by counting-statistics ('shot noise') of $\sigma = 3 \cdot 10^3$ cps (for one second integrations). This is combined with the Johnson-Nyqvist noise of the detector (10^{11} Ω amplifier), which is around $6 \cdot 10^3$ cps for 1 second integrations. Therefore, the expected standard error limit for the entire acquisition is 0.01%, which is achieved routinely.

In the long method (Figure 6), δD is acquired in high-resolution mode with a typical $^{12}CH_3D$ intensity of around $6 \cdot 10^4$ cps, which leads to shot noise limit of $\sigma = 2 \cdot 10^2$ cps for one second integrations, while the dark-noise and scattered-ion noise contributions from the ion counter (CDD) are negligible (<0.1cps). For this measurement, the expected standard error limit is 0.12‰ for the entire acquisition, which is achieved routinely.

In the short method (Figure 6), δD is acquired at a typical $^{12}CH_3D$ intensity of around $5 \cdot 10^5$ cps, which leads to a shot noise limit of $\sigma = 7 \cdot 10^2$ cps for one second integrations. This combined with the Johnson-Nyqvist noise of the detector (10^{12} Ω amplifier) of 10^3, results in an expected standard error of 0.15‰ for the entire acquisition, which is achieved routinely.

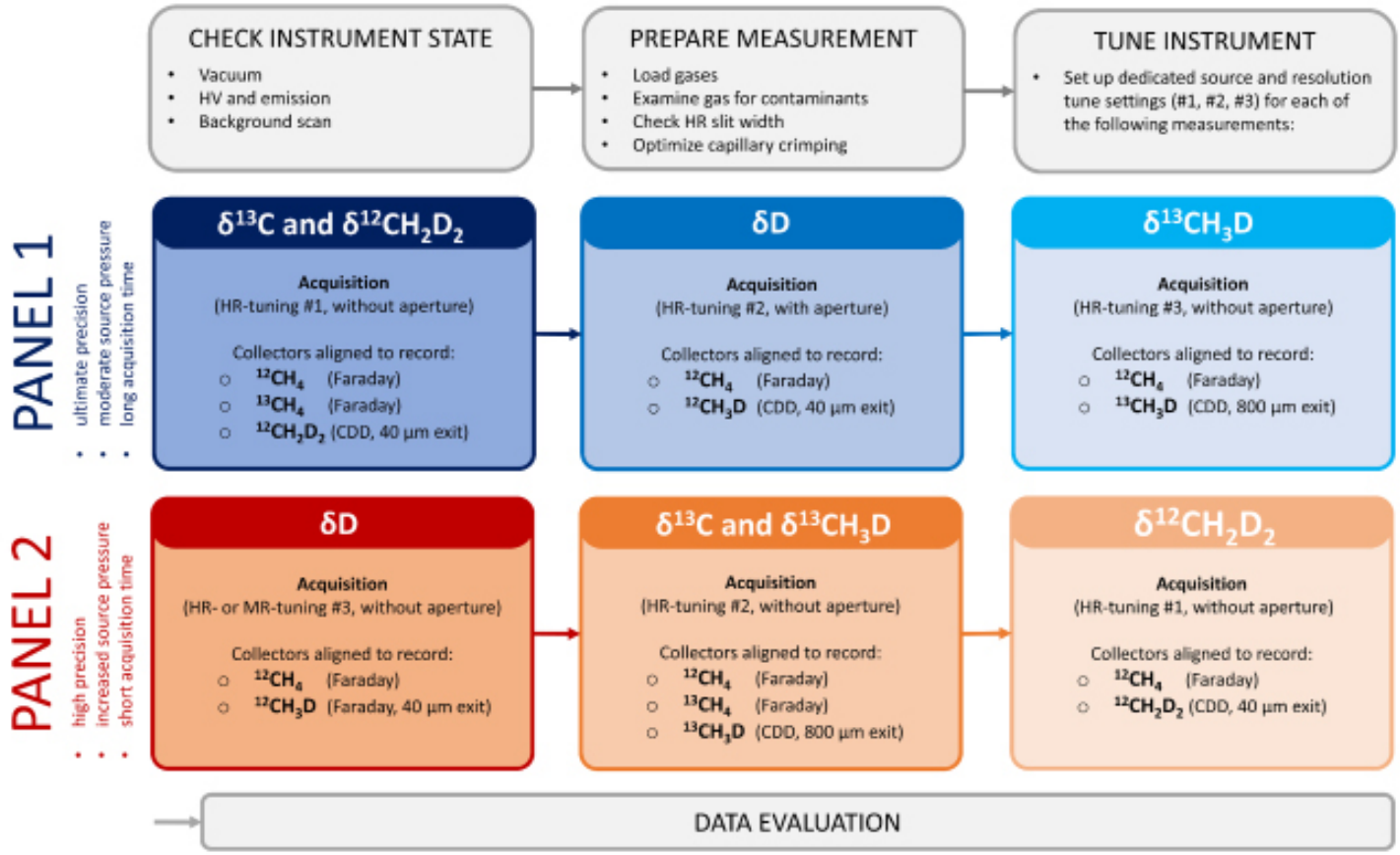

Figure 6: Example of a measurement strategy to observe the full inventory of unsubstituted, singly substituted and doubly substituted ('clumped') methane isotopologues. Panel 1: a long method devised for ultimate precision analysis at a rate of 1 sample per two days at moderate source pressures; Panel 2: a shorter method devised for analysis at a rate of 1 samples per day, at modestly degraded precision and higher source pressures.

$\delta^{13}CH_3D$ is acquired with a typical $^{13}CH_3D$ intensity of $5{\cdot}10^3$ cps, resulting in shot noise of $\sigma=7{\cdot}10^1$ cps, with negligible dark-noise and scattered-ion noise from the CDD (<0.1cps). The expected standard error limit is 0.28‰ for the entire acquisition, which is achieved routinely.

$\delta^{12}CH_2D_2$ is acquired with a typical $^{12}CH_2D_2$ intensity of $1{\cdot}10^2$ cps, resulting in shot noise of $\sigma=1{\cdot}10^1$ cps, with negligible dark-noise and scattered-ion noise from the CDD (<0.1cps). The expected standard error limit is 1‰ for the entire acquisition, which is achieved routinely.

Three different Ultra HR-IRMS laboratories, in which the bulk and clumped isotope inventory of methane is independently analyzed (UC Berkeley, Tokyo Institute of Technology, Caltech), report consistent analytical performance (Table 3).

Table 3: Overview of typical accuracy and precision as achieved in different Ultra HR-IRMS laboratories (University of California, Berkeley; Tokyo Institute of Technology; California Institute of Technology).

		Shot noise limit (s. text)	UC Berkeley*	Tokyo Tech	Caltech
Internal precision (1 s.e.)	$\delta^{13}C$	±0.01‰	±0.01‰	±0.01‰	±0.01‰
	δD	±0.12‰	±0.12‰	±0.11‰	±0.12‰
	$\delta^{13}CH_3D$	±0.28‰	±0.25‰	±0.35‰	±0.28‰
	$\delta^{12}CH_2D_2$	±1.00‰	±1.35‰	±1.35‰	±1.10‰
External reproducibility (1 s.d.)	$\delta^{13}C$		±0.02‰	±0.03‰	±0.03‰
	δD		±0.15‰	±0.09‰	±0.20‰
	$\Delta^{13}CH_3D$		±0.33‰	±0.31‰	±0.35‰
	$\Delta^{12}CH_2D_2$		±1.35‰	±1.24‰	±1.22‰

*Eldridge et al. (2019)

Internal precision is assessed by zero enrichment measurements. After a total measurement duration of about 18 hours, the standard error (1 s.e.= σ/√n) of $\delta^{12}CH_2D_2$ approaches the 1‰ line (Figure 7). A standard error of 2‰ is achieved after ~7 hours. Note that the intensity of $^{12}CH_2D_2$ is 50 cps in this example, which is lower than is typical when measuring unknowns.

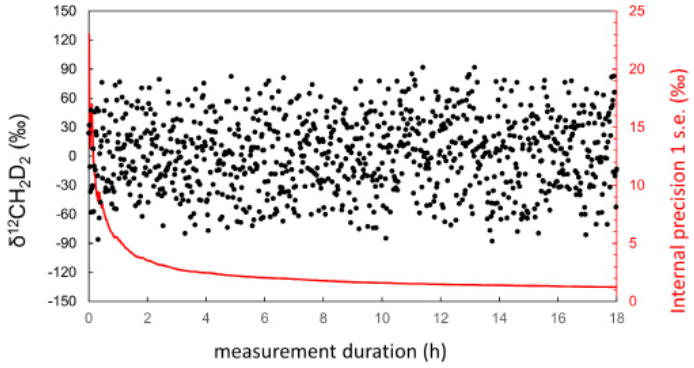

Figure 7: Zero enrichment measurement of $\delta^{12}CH_2D_2$ in the Bremen factory (intensity of $^{12}CH_2D_2$ is 50 cps): a standard error of ~1‰ is approached after 18 hours total measurement duration (including valve switching equilibration times, repeated pressure adjustments, and peak centering).

External precision is determined by periodically measuring a laboratory standard. The external precision incorporates potential error caused by instability of ion source, mass analyzer and detector, plus isotope fractionation associated with gas extraction and/or pernicious contaminants (H_2O, N_2, CO, etc.). Therefore, routine measurement of a lab standard helps evaluating the external precision as well as monitoring instrument condition. Figure 8 shows that $\Delta^{12}CH_2D_2$ results of a lab standard in the Caltech lab are stable over a six-month session, and the external precision based on the standard deviation of these results are only slightly larger (1.29 ‰) than internal precision (Table 3).

Scientific application

We close this note with brief illustrations of three geochemical uses of methane clumped isotope measurements. These case studies draw on Ultra HR-IRMS measurements (most not yet published in the peer reviewed literature) of $\delta^{13}C$, δD, $\Delta^{13}CH_3D$ and $\Delta^{12}CH_2D_2$ of methane extracted from natural gases and laboratory experiments, taken from recent work at Caltech and the University of California, Berkeley.

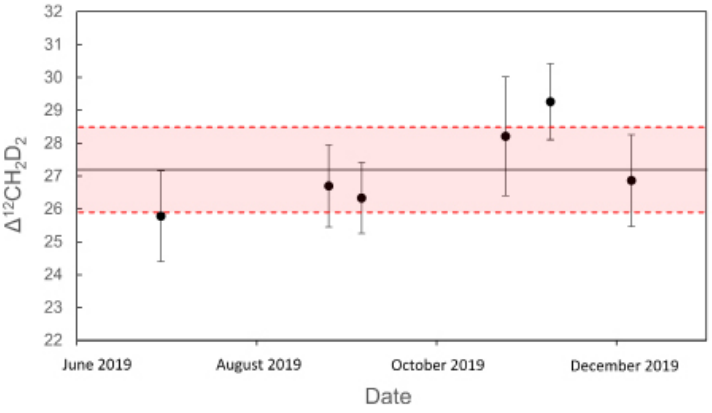

Figure 8: Long term reproducibility for laboratory (house) standard gas during a six-month session in the Caltech laboratory. Average (black solid line) and 1 s.d. error envelope (shaded).

Forensic discrimination: A simple but important purpose of stable isotope ratio measurements of methane is forensic assignment of natural samples to specific formation mechanisms. As was noted above and illustrated in Figure 1, this is challenging because of overlap in isotopic properties of methane types, and the potential that natural samples are mixtures of two or more sources. The expansion of the number of analyzed dimensions from two ($\delta^{13}C$ and δD) to four (plus $\Delta^{13}CH_3D$ and $\Delta^{12}CH_2D_2$) improves the forensic specificity of stable isotope ‚fingerprinting'. The full expression of this capability can only be understood by considering all four independent dimensions, and therefore is not easy to intuit. Figure 9 illuminates how this approach can be especially effective, where low-maturity thermogenic methane — a type characterized by intermediate $\delta^{13}C$ and δD and thus hard to distinguish using Figure 1 alone — can be recognized by its exceptionally low $\Delta^{12}CH_2D_2$ values at $\delta^{13}C$ values of -60 to -45‰.

Formation mechanism: Methane clumped isotope can provide insights into the mechanisms of formation, particularly where formation involves a non-equilibrium isotope effect that is diagnostic of the relevant substrates or chemistry. In one such study, illustrated in Figure 10, Dong et al. (submitted) performed pyrolysis experiments on n-octadecane ($C_{18}H_{38}$), an oil-analog aliphatic compound. The $\Delta^{13}CH_3D$ values of product methane are relatively close to equilibrium at the experimental temperature (400 ˚C), whereas $\Delta^{12}CH_2D_2$ values are 30 to 40‰ lower than expected for equilibrium. The large deficit in $\Delta^{12}CH_2D_2$ can be explained by sourcing hydrogen in a methane

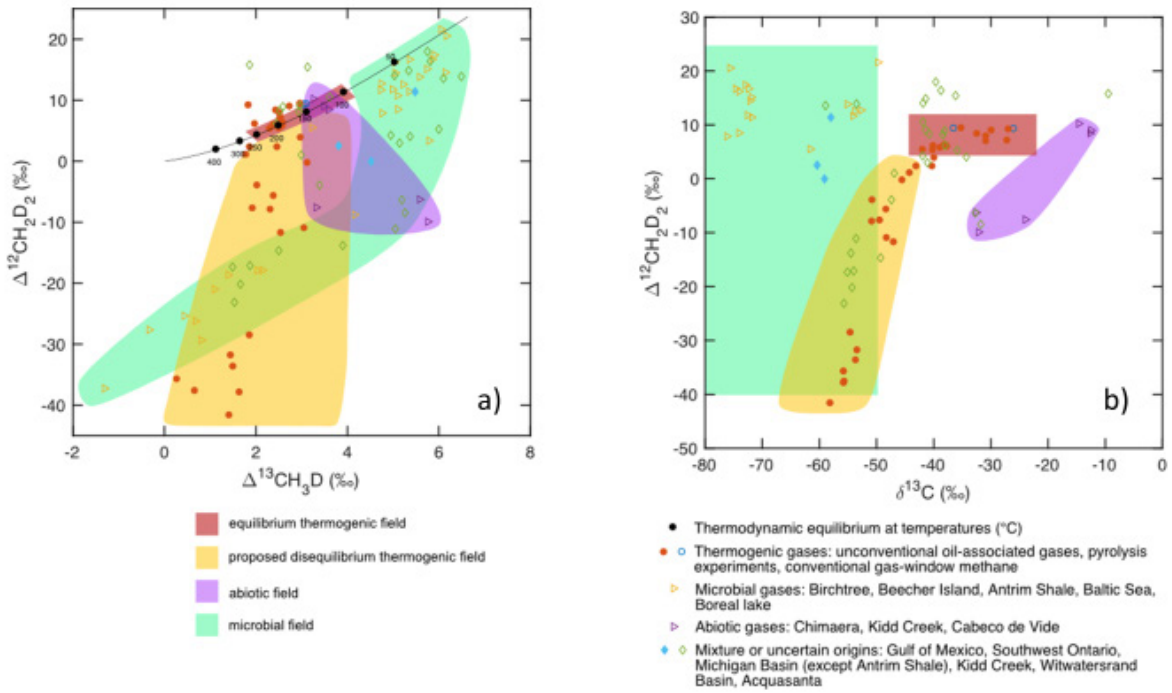

Figure 9: Diagrams of (a) $\Delta^{13}CH_3D$ - $\Delta^{12}CH_2D_2$ and (b) $\delta^{13}C$ - $\Delta^{12}CH_2D_2$ with forensically diagnostic fields. Data from Young et al. (2017), Giunta et al. (2019), Ash et al. (2019), Young et al. (2019), Thiagarajan et al. (2020b), Dong et al. (submitted) and Xie et al. (in preparation), measured on Ultra HR-IRMS (filled symbols) and other HR-IRMS (open symbols).

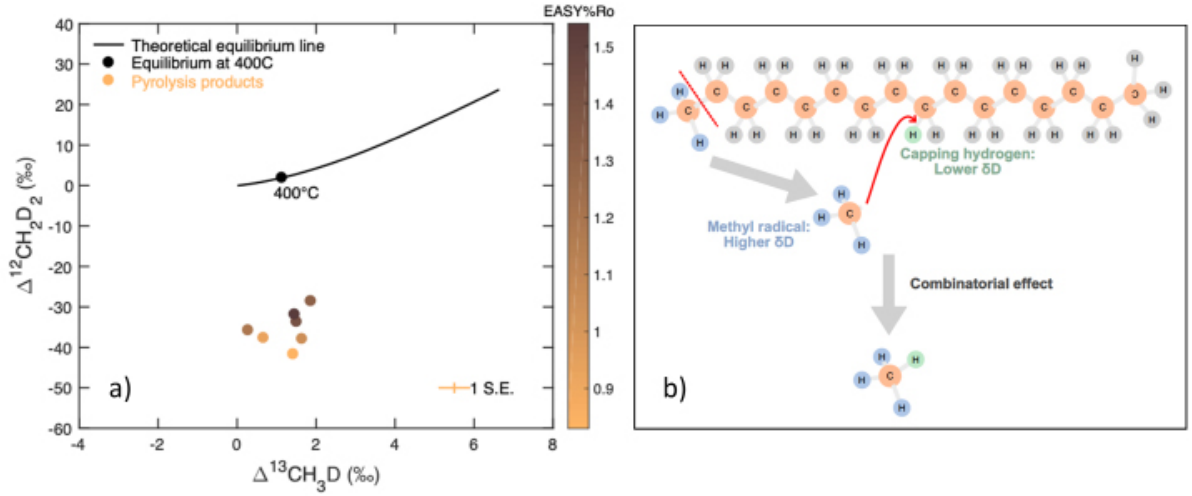

Figure 10: Panel a: Clumped-isotope compositions of methane generated in pyrolysis of n-octadecane. The data points for pyrolysis products are color-coded by their thermal maturities, as measured by the EASY%R0 index (Sweeney and Burnham, 1990); darker tones indicate higher thermal maturities (i.e., longer heating times). The solid line shows the thermodynamic equilibrium $\Delta^{13}CH_3D$ and $\Delta^{12}CH_2D_2$ values from 2000 to 0°C. The equilibrated value at the experimental temperature (400 ˚C) is marked as a black dot. The $\Delta^{13}CH_3D$ values of methane products are within 2 standard errors (2 s.e.) of the expected equilibrium composition whereas the $\Delta^{12}CH_2D_2$ values are much more depleted than equilibrium and do not correspond to any possible temperature. And the $\Delta^{12}CH_2D_2$ values are gradually approaching equilibrium value with maturation. Analytical error within symbol size.
Panel b: A cartoon of the chemical mechanism of methane generation in pyrolysis of n-octadecane; see text for details.

molecule from pools with different isotope compositions, previously referred to as a 'combinatorial effect' (right panel of Figure 10). Specifically, methane generation starts by producing a methyl radical by breaking a carbon—carbon bond through homolytic cleavage or beta scission. Then the methyl radical attacks n-octadecane and extracts a capping hydrogen. Once the product methane forms, the four hydrogen atoms are symmetrically equivalent, but three hydrogen atoms from the methyl radical has a higher δD, whereas the fourth capping hydrogen has a lower δD. The symmetric equivalence of the four hydrogen atoms will lead one to predict a stochastic abundance of $^{12}CH_2D_2$ that is much higher than the true probability of randomly forming $^{12}CH_2D_2$ – this phenomenon is the 'combinatorial effect'. This effect happens in assembling hydrogen from isotopically different pools, causing deficit in $\Delta^{12}CH_2D_2$ but only subtly affecting $\Delta^{13}CH_3D$. This finding provides an isotopic fingerprint for thermogenic methane formed in the early, strongly irreversible and kinetically controlled steps of catagenesis; it also demonstrates that non-equilibrium clumped isotope signatures are not unique to microbial or abiotic methane, as has been previously suggested, but also occur in high temperature catagenetic chemistry.

Geothermometry: Methane formed in several natural settings often has a clumped isotope composition close to equilibrium at its environmental temperature; common examples include thermogenic natural gases from thermally mature source rocks, microbial gases in sub-surface settings where net methane accumulation is relatively slow, and hydrothermal vent fluids. Measurements of $\Delta^{13}CH_3D$ and $\Delta^{12}CH_2D_2$ on the same sample allow one to test whether a sample's clumped isotope composition is consistent with mutual equilibrium among all of the measured isotopologues, in which case the sample should fall within error of the calibrated equilibrium curve in Figure 11. When methane is in equilibrium with respect to its clumped isotope abundances, the Δi values can serve as temperature proxies, with accuracy and precision on the order of 10's of degrees at catagenetic and hydrothermal temperatures down to several degrees at near-earth-surface temperatures. Previous work also suggests that methane can preserve formation temperatures through later geological history, up to storage temperatures as high as ~250-300 ˚C. This tool is tremendously useful for the study of methane from sub-surface fluids because it allows one to assign a usefully precise geophysical temperature to a formation process (unlike qualitative proxies such as bulk

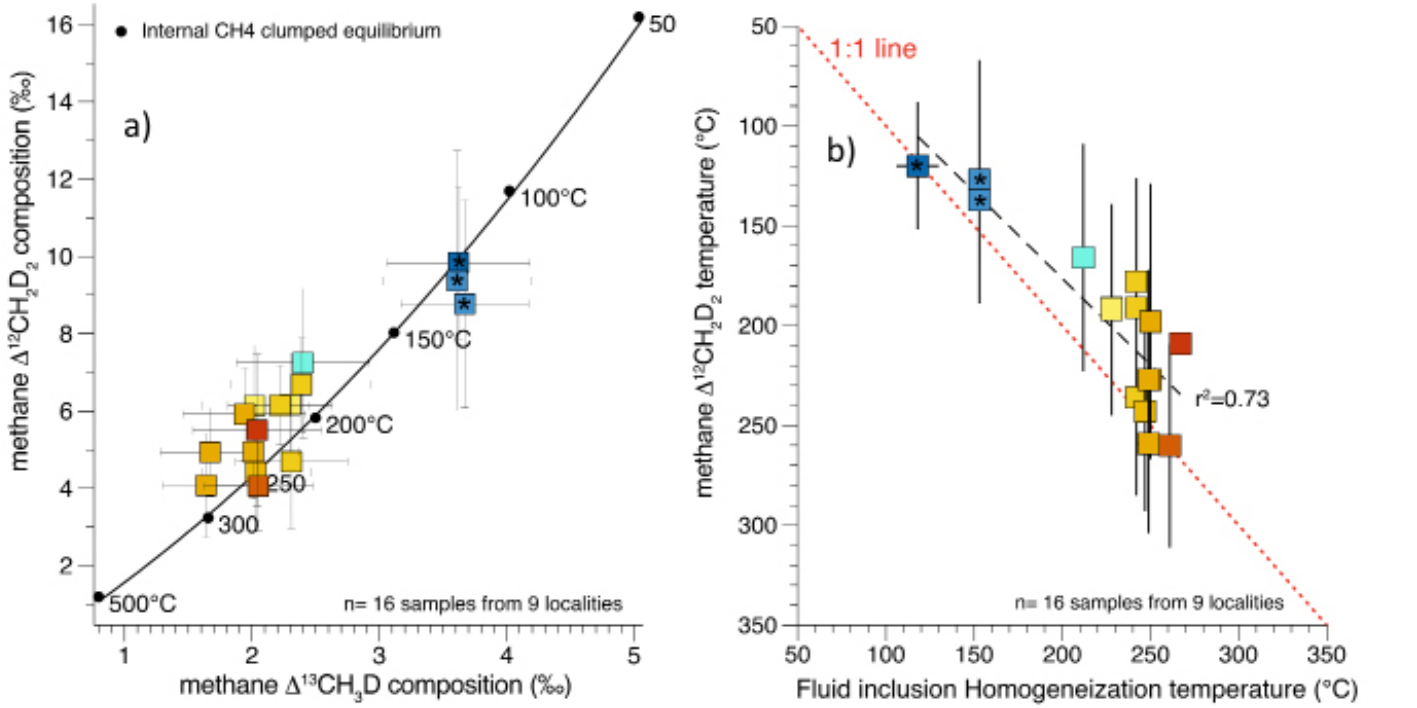

Figure 11: Plot of $\Delta^{12}CH_2D_2$ vs. $\Delta^{13}CH_3D$ values measured on CH_4 liberated from Alpine fluid inclusions (a) and comparison with clumped isotope temperatures to independently determined fluid inclusion homogenization temperatures (b); the 1:1 line is show for reference; data are from Mullis et al. 2017). Samples are consistent with equilibrium clumped isotope distributions (curve on left panel) at the temperatures of inclusion trapping (1:1 line on right panel).

C isotope composition, which generally only allow one to rank-order thermal maturities of related gases). Figure 11 presents the results of an application of the methane clumped isotope geothermometer to fluid inclusions from tectonic quartz veins in the Alps (Mangenot et al., in prep.). Thermogenic methane in these inclusions has clumped isotope compositions indicating intramolecular isotopic equilibrium at catagenetic to low-grade (sub-greenschist) metamorphic temperatures ($T\Delta^{13}CH_3D$: 120-300 °C; $T\Delta^{12}CH_2D_2$ = 120-260 °C), and provide direct evidence of large reservoirs of thermogenic methane trapped beneath the Alps during Mid-Miocene tectonic nappe emplacement.

Acknowledgements

We thank the ExxonMobil Upstream Research Company, Petrobras, and Shell for providing samples and sponsored research support that contributed to data in Figures 1, and 9 — 11, and to Caltech and the US Department of Energy for providing financial and material support for measurements described here. We also thank our co-authors on papers cited in the Reference section for their contributions to the creation and interpretation of data reproduced here.

References

1. Ash, J.L., Egger, M., Treude, T., Kohl, I., Cragg, B., Parkes, R.J., Slomp, C.P., Sherwood Lollar, B., Young, E.D. (2019) Exchange catalysis during anaerobic methanotrophy revealed by $^{12}CH_2D_2$ and $^{13}CH_3D$ in methane. Geochemical Perspectives Letters, 10, 26-30.
2. Dong, G., Xie, H., Kitchen, N., Formolo, M., Lawson, M., Sessions, A. and Eiler, J. (2020) Methane Clumped Isotope Effects during Hydrocarbon Cracking in Laboratory Experiments. Submitted to Geochimica et Cosmochimica Acta.
3. Douglas, P.M., Stolper, D.A., Eiler, J.M., Sessions, A.L., Lawson, M., Shuai, Y., & Niemann, M. (2017). Methane clumped isotopes: progress and potential for a new isotopic tracer. Organic Geochemistry, 113, 262-282.
4. Eiler (2007) "Clumped-isotope" geochemistry – The study of naturally-occurring, multiply substituted isotopologues. Earth and Planetary Science Letters, 262, 309–327.
5. Eldridge, D.L., Korol, R., Lloyd, M.K., Turner, A.C., Webb, M.A., Miller, T.F., Stolper, D.A. (2019) Comparison of Experimental vs Theoretical Abundances of 13CH3D and $^{12}CH_2D_2$ for Isotopically Equilibrated Systems from 1 to 500 °C. ACS Earth and Space Chemistry, 3, 2747–2764.
6. Etiope, G., Sherwood Lollar, B. (2013) Abiotic methane on Earth. Reviews of Geophysics, 51, 276–299.
7. Etiope, G. (2015) Natural Gas Seepage: The Earth's Hydrocarbon Degassing. Springer, Cham, Switzerland.
8. Giunta, T., Young, E.D., Warr, O., Kohl, I., Ash, J.L., Martini, A., Mundle, S.O.C., Rumble, D., Pérez-Rodríguez, I., Wasley, M., LaRowe, D.E., Gilbert, A., Sherwood Lollar, B. (2019) Methane sources and sinks in continental sedimentary systems: New insights from paired clumped isotopologues $^{13}CH_3D$ and $^{12}CH_2D_2$. Geochimica et Cosmochimica Acta, 245, 327–351.
9. Mangenot et al. (in preparation)
10. Milkov, A. V., and Etiope, G. (2018). Revised genetic diagrams for natural gases based on a global dataset of > 20,000 samples. Organic Geochemistry, 125, 109-120.
11. Mullis, J., Mählmann, R. F. and Wolf, M. (2017) Fluid inclusion microthermometry to calibrate vitrinite reflectance (between 50 and 270 °C), illite Kübler-Index data and the diagenesis/anchizone boundary in the external part of the Central Alps. Appl. Clay Sci., 143, 307–319.
12. Schoell, M. (1980) The hydrogen and carbon isotopic composition of methane from natural gases of various origins. Geochimica et Cosmochimica Acta 44, 649–661.
13. Sherwood, O. A., Schwietzke, S., Arling, V. A., and Etiope, G.: Global Inventory of Gas Geochemistry Data from Fossil Fuel, Microbial and Burning Sources, version 2017, Earth Syst. Sci. Data, 9, 639–656, https://doi.org/10.5194/essd-9-639-2017, 2017.
14. Stolper, D.A., Sessions, A.L., Ferreira, A.A., Santos Neto, E.V., Schimmelmann, A., Shusta, S.S., Valentine, D.L., Eiler, J.M. (2014a) Combined 13C-D and D-D clumping in methane: Methods and preliminary results. Geochimica et Cosmochimica Acta, 126, 169–191.
15. Stolper, D. A., Lawson, M., Davis, C. L., Ferreira, A. A., Neto, E. V. S., Ellis, G. S., Lewan, M. D., Martini, A. M., Tang, Y., Schoell, M., Sessions, A. L. and Eiler, J. M. (2014b) Formation temperatures of thermogenic and biogenic methane. Science, 344, 1500–1503.
16. Sweeney, J.J. and Burnham, A.K. (1990) Evaluation of a simple Model of Vitrinite Reflectance based on Chemical Kinetics. AAPG Bulletin, 74, 1559-1570.
17. Thiagarajan, N., Xie, H., Ponton, C., Kitchen, N., Peterson, B., Lawson, M., Formolo, M., Xiao, Y., and Eiler, J. (2020a) Isotopic evidence for quasi-equilibrium chemistry in thermally mature natural gases. Proceedings of the National Academy of Sciences, 117(8), 3989-3995, doi:10.1073/pnas.1906507117
18. Thiagarajan, N., Kitchen, N., Xie, H., Ponton, C., Lawson, M., Formolo, M. and Eiler, J. (2020b) Identifying thermogenic and microbial methane in deep water Gulf of Mexico Reservoirs. Geochimica et Cosmochimica Acta 275, 188–208.
19. Whiticar, M.J. (1990) Carbon and hydrogen isotope systematics of bacterial formation and oxidation of methane. Chemical Geology, 161(1-3), 291-314.
20. Xie et al. (2020) The evolution of intra- and inter-molecular isotope equilibria in natural gases with thermal maturation, (in preparation).
21. Young, E.D., Kohl, I.E., Sherwood Lollar, B., Etiope, G., Rumble, D., Li, S., Haghnegahdar, M.A., Schauble, E.A., McCain, K.A., Foustoukos, D.I., Sutclife, C., Warr, O., Ballentine, C.J., Onstott, T.C., Hosgormez, H., Neubeck, A., Marques, J.M., Pérez-Rodríguez, I., Rowe, A.R., LaRowe, D.E., Magnabosco, C., Yeung, L.Y., Ash, J.L., Bryndzia, L.T. (2017) The relative abundances of resolved $^{12}CH_2D_2$ and $^{13}CH_3D$ and mechanisms controlling isotopic bond ordering in abiotic and biotic methane gases. Geochimica et Cosmochimica Acta, 203, 235–264.
22. Young E.D. (2019) A two-dimensional perspective on CH_4 isotope clumping: Distinguishing process from source. In B. Orcutt, I. Daniel, and R. Dasgupta (Eds.) Deep Carbon: Past to Present, (pp. 388-414), Cambridge: Cambridge University Press, doi:10.1017/9781108677950.013.